

# Evolution-guided engineering of small-molecule biosensors

Tim Snoek<sup>1</sup>, Evan K. Chaberski<sup>1</sup>, Francesca Ambri<sup>1</sup>, Stefan Kol<sup>1</sup>, Sara P. Bjørn<sup>1</sup>, Bo Pang<sup>2</sup>, Jesus F. Barajas<sup>2</sup>, Ditte H. Welner<sup>1</sup>, Michael K. Jensen<sup>1\*</sup> & Jay. D Keasling<sup>1-5</sup>

<sup>1</sup> Novo Nordisk Foundation Center for Biosustainability, Technical University of Denmark, Kgs. Lyngby, Denmark

<sup>2</sup> Joint BioEnergy Institute, Emeryville, CA, USA

<sup>3</sup> Biological Systems and Engineering Division, Lawrence Berkeley National Laboratory, Berkeley, CA, USA

<sup>4</sup> Department of Chemical and Biomolecular Engineering & Department of Bioengineering, University of California, Berkeley, CA, USA

<sup>5</sup> Center for Synthetic Biochemistry, Institute for Synthetic Biology, Shenzhen Institutes of Advanced Technologies, Shenzhen, China

\* To whom correspondence should be addressed. Michael K. Jensen: Email: [mije@biosustain.dtu.dk](mailto:mije@biosustain.dtu.dk), Tel: +45 6128 4850

## Abstract

Allosteric transcription factors (aTFs) have proven widely applicable for biotechnology and synthetic biology as ligand-specific biosensors enabling real-time monitoring, selection and regulation of cellular metabolism. However, both the biosensor specificity and the correlation between ligand concentration and biosensor output signal, also known as the transfer function, often needs to be optimized before meeting application needs. Here, we present a versatile and high-throughput method to evolve and functionalize prokaryotic aTF specificity and transfer functions in a eukaryote chassis, namely baker's yeast *Saccharomyces cerevisiae*. From a single round of directed evolution of the effector-binding domain (EBD) coupled with various

toggled selection regimes, we robustly select aTF variants of the *cis*, *cis*-muconic acid-inducible transcription factor BenM evolved for change in ligand specificity, increased dynamic output range, shifts in operational range, and a complete inversion of function from activation to repression. Importantly, by targeting only the EBD, the evolved biosensors display DNA-binding affinities similar to BenM, and are functional when ported back into a non-native prokaryote chassis. The developed platform technology thus leverages aTF evolvability for the development of new host-agnostic biosensors with user-defined small-molecule specificities and transfer functions.

## Introduction

The ability to selectively control gene expression has fueled synthetic biology as an engineering discipline. Ever since the description of genetic systems inducible by small molecules, such as IPTG, arabinose or tetracycline<sup>1</sup>, the repertoire of genetic switches for ligand-induced control of gene expression has vastly expanded, targeting diverse applications, including directed evolution of bio-based microbial production, *in situ* diagnosis of human gut microbiota, conditional control of mammalian cell differentiation, and synthetic cell-cell communication devices<sup>2-5</sup>.

Given the large number of allosteric transcription factors (aTFs) present in the prokaryotic kingdom<sup>6</sup>, the diversity of chemical structures recognized<sup>7</sup>, and their modular domain structure encoded by a conserved DNA-binding domain (DBD) linked to a diversified effector-binding domain (EBD)<sup>8</sup>, small-molecule biosensors based on aTFs are a particularly valuable class of genetic switches. Ongoing biosensor research therefore seeks to prospect new biosensors from genomic resources<sup>9,10</sup>, while also developing general design rules and engineering strategies

57 from existing aTFs. Indeed, due to the modular structure of aTFs, several studies  
58 have successfully adopted EBD-swapping strategies into platform DBDs to rationally  
59 engineer new aTF logic<sup>11–13</sup>, while engineering EBD destabilization for ligand-  
60 controlled biosensor stability also have proven successful<sup>14–16</sup>. However, these  
61 rational design strategies for engineering new biosensors suffer from the introduction  
62 of cross-talk between ligand specificities, difficulty in creating chimeras from different  
63 aTF superfamilies, and the risk of losing allostery<sup>2,11,17</sup>. Ultimately, this may impact  
64 several aspects of biosensor performance, such as the operational and dynamic  
65 output ranges, the specificity, and mode-of-action - collectively referred to as the  
66 biosensor transfer function or logic.

67 Acknowledging that allosteric regulation relies on complex interdomain  
68 interactions, studies beyond pure rational engineering have successfully adopted  
69 directed evolution based on global and randomised mutagenesis approaches for  
70 engineering new aTF logic. For instance, the dynamic range of aTFs, i.e. the  
71 quantitative relationship between small-molecule inducer concentration and  
72 biosensor output signal, has been optimized by directed evolution to match biosensor  
73 performance to the experimental design and application needs<sup>18</sup>. Likewise, when no  
74 available biosensor exists to the ligand of interest, attempts on both randomised and  
75 structure-guided directed evolution of new biosensor specificities and improved  
76 operational ranges from existing aTFs have also been successfully demonstrated<sup>19–</sup>  
77 <sup>22</sup>. Moreover, starting from allosterically-dead aTF variants with constitutive DNA-  
78 binding, semi-structure-guided mutagenesis has been used to identify and evolve  
79 new biosensors with changes in both dynamic output range and inversion of function  
80 (ie. inverse-repression)<sup>23–25</sup>. In most of these library studies, the mutagenized aTF  
81 libraries were characterized based on ligand-induced expression of fluorescent  
82 reporter genes or antibiotic resistance genes for multiplexed selection of aTF variants  
83 responding to the ‘trait’ of interest using biosensor readouts based on fluorescence-  
84 activated cell sorting (FACS) or cell survival, respectively.

85           Even though transfer functions and specificities can be optimized using  
86   directed evolution and high-throughput read-outs, mutagenizing allosteric proteins is  
87   known to cause abundant loss-of-function mutants related specifically to residues  
88   involved in ligand binding and those required for maintaining aTF structures<sup>26,27</sup>.  
89   Likewise, when mutating aTFs, trade-offs between transfer function parameters are  
90   frequently observed, such as variants with increased dynamic output ranges are  
91   diluted by aTF variants in a constitutive allosterically active state<sup>24</sup>. For this reason  
92   several studies have further adopted toggled selection regimes with both positive  
93   (ON) and negative (OFF) selection regimes to robustly evolve aTFs with user-defined  
94   changes in small-molecule specificity<sup>27,28</sup>, changes in dynamic and operational  
95   ranges<sup>29</sup>, and inversion of function<sup>30</sup>. Such toggled selection regimes can  
96   successfully limit, or completely abolish, aTF variants with unintended trade-offs in  
97   transfer functions or ligand cross-reactivity. Also, as biosensor library sizes are  
98   typically limited by the transformation efficiency, the power of directed evolution  
99   enables identification of beneficial aTF mutations to accumulate over iterative rounds  
100   of screening from even relatively small library sizes<sup>31</sup>.

101           Still, no single strategy has demonstrated the evolvability of multiple transfer  
102   function parameters and specificity from one existing aTF. Likewise, for all the  
103   studies on engineering prokaryotic aTFs as biosensors based on directed evolution,  
104   there is no evidence available for the portability of engineered aTFs as functional  
105   biosensors between different host organisms<sup>19,22–24,27,30,32</sup>. From both an engineering  
106   and an application point of view, the demonstration of sequence-identifiers related to  
107   defined transfer function parameters and specificity, and aTF portability between  
108   different hosts is of broad interest for biotechnology and human health applications<sup>7</sup>.

109           Here, we present a simple and high-throughput method to generate tailor-  
110   made aTF biosensors with novel transfer function parameters and specificities by  
111   means of a single round of directed evolution coupled to stringent FACS-based  
112   toggled selection regimes. Selected archetypical aTF variants display complete



113 affinity-maturation towards a non-cognate ligand, 15-fold increased dynamic output  
114 range, a 40-fold shift in operational range, and inversion of function from ligand-  
115 induced activation to repression, compared to parental aTF. Furthermore, we  
116 sequenced and further characterized selected aTF variants by kinetic analyses and  
117 functional studies in order to pinpoint mutations linked to changes in functionality,  
118 thereby enabling the identification of mutational hotspots for defined transfer function  
119 parameters. The presented method leverages aTF evolvability, and supports the  
120 high-throughput development of new biosensors with user-defined small-molecule  
121 specificities and transfer functions. Finally, the demonstration that evolved aTF  
122 variants can be ported back into bacteria as functional biosensors underscores the  
123 general usability of the method for biosensor development for a wide range of hosts.

124

## 125 **Results**

126

### 127 *Experimental design and biosensor variant library construction*

128 In order to establish a method for the development of new genetically-  
129 encoded biosensors based on allosterically regulated transcription factors (aTFs)  
130 with user-defined functionalities, we deployed directed evolution coupled with toggled  
131 selection using fluorescence-activated cell sorting (FACS)(Fig. 1A). As for transfer  
132 function parameters, we focused on evolving biosensors with quantitative changes in  
133 dynamic and operational ranges, qualitative changes related to inversion of function,  
134 as well as change of small-molecule specificity. These are frequently targeted  
135 parameters in biosensor optimization (Fig. 1B). Furthermore we chose to  
136 demonstrate the method in yeast because i) the number of biosensors implemented  
137 in yeast, and other eukaryotes, is small as compared to the plethora of ligand-  
138 sensing systems available in prokaryotes<sup>7,33</sup>, and ii) using yeast allowed us to  
139 leverage high efficiency of homologous recombination for library generation through  
140 plasmid gap repair<sup>18,34</sup>.

141 As a proof-of-concept, we used a randomised variant library of the LysR-type  
 142 *Acinetobacter* sp. ADP1 *cis,cis*-muconic (CCM) acid-binding transcriptional activator  
 143 BenM, previously engineered as biosensor in the budding yeast *Saccharomyces*  
 144 *cerevisiae*<sup>18</sup>. For the aTF variant library generation we considered several aspects in  
 145 order to generate a high-quality aTF mutant library useful for selection of variants  
 146 with both changes in transfer function parameters and specificity. First, in order to  
 147 limit the loss of allostery due to interdomain interactions and to bias the selection  
 148 towards aTF variants with intact DNA-binding specificity maintained, we specifically  
 149 focused on evolving the sequence-diverse aTF effector-binding domain (EBD)(Fig.  
 150 1A). Next, since we aimed to uncover variants with either quantitative (operational  
 151 and dynamic ranges) or qualitative (specificity and inversion of function) changes in  
 152 functionality, we hypothesized a library spanning a variation in mutational loads  
 153 would be most useful, and therefore created the aTF library consisting of approx  
 154 85,000 variants generated from amplicon pools of 2-5 rounds of error-prone PCR  
 155 (epPCR) targeting the non-conserved EBD residues 73-305 of BenM (Fig. 1A, Suppl.  
 156 Fig. S1)(see Methods).

157 For the evolution set-up, the diversified EDB templates were co-transformed  
 158 with a linearized plasmid backbone encoding the BenM WT DBD, into a platform  
 159 yeast strain expressing GFP from an engineered weak *CYC1* promoter harboring a  
 160 previously described aTF binding site (*aTF-O pro*)<sup>18</sup> to allow for library construction  
 161 by gap repair and aTF-controlled inducible expression of GFP, respectively (Fig. 1A).  
 162 For all designs, we genomically integrated *aTF-O::GFP* as a single reporter copy.  
 163 Next, this library was subjected to various user-defined FACS-based toggled  
 164 selection regimes in order to evolve aTF variants with new ligand specificity,  
 165 extended operational and dynamic ranges, and inversion of function (Fig 1A-B). In  
 166 general first- and second-round sorting included 0.0032 - 5.4% and 34.9 - 43.4% of  
 167 the library, respectively, depending on the trait sought for (Suppl. Table S1).

168 Finally, variants evolved in this study were sequenced (including promoter  
169 and terminator) and subsequently independently re-transformed into clean yeast  
170 background strains, before being re-phenotyped to rule out phenotypic effects of  
171 potential secondary genomic mutations.

172

### 173 *Evolution-guided engineering of biosensor transfer function and specificity*

174 The first transfer function parameter to be improved was dynamic range. To  
175 this end, we first sorted BenM variants that specifically showed high fluorescent  
176 levels in the presence of 1.4 mM CCM (ON state)(Fig. 1B, Fig. 2A, and Suppl. Table  
177 S1), a concentration we previously reported relevant for screening in yeast cells<sup>18</sup>.  
178 Next, we performed a second round of sorting to remove variants with high  
179 background fluorescence in the absence of inducer (OFF state) by sorting variants  
180 that did not display background fluorescence under uninduced conditions. Indeed,  
181 comparing mean fluorescence intensities of clonal variants isolated after one or two  
182 rounds of sorting showed that our toggled selection yielded 62 variants with both  
183 lower OFF state (mean OFF state decreased from 4.0 +/- 3.1 to 1.3 +/- 0.6) and  
184 higher fold induction (mean fold-induction increased from 4.4 +/- 3.1 to 9.0 +/- 6.1)  
185 upon ligand administration as compared to a single round of positive selection (Fig.  
186 2A). More specifically, by sorting 0.17% and 43.4% of our library in ON and OFF  
187 states, respectively, we found that 83/94 (88%) of clonal variants obtained after  
188 toggled selection improved induction at 1.4 mM CCM with a maximum of 38-fold  
189 induction, compared to 2.8-fold induction of BenM WT (Fig. 2A).

190 Next, we sought to use directed evolution and toggled selection for affinity-  
191 maturation of BenM for new ligand specificity towards adipic acid, a hydrogenated  
192 and chemically divergent ligand commercially used in chemical, food and  
193 pharmaceutical industries<sup>35</sup>. When engineering new aTF biosensor specificity, it is  
194 important to acknowledge that relaxation of ligand specificity towards cognate ligands  
195 can impose a challenge in maintaining allostery in transcriptional regulators<sup>16</sup>, and

for this reason engineering specificity requires both negative selection (ie. loss of specificity for the native ligand) and positive selection (ie. gain of specificity for the new ligand)<sup>28,36</sup>. Hence, similar to evolving dynamic range variants, we carried out a toggled selection procedure using adipic acid as an inducer in the ON state, and subsequently sorting variants without background fluorescence under uninduced conditions (OFF state)(Fig. 2B). As we observed when we analyzed clonal variants for changes in dynamic range, we found that the toggled selection procedure reduced the OFF state from a mean value of 4.2 +/- 3.5 to 1.2 +/- 0.6 compared to a single round of positive selection (Fig. 2B). For the affinity-matured variants we found that by sorting 0.032% and 40.5% of our library in ON and OFF states, respectively, a total of 36/44 (82%) clonal variants obtained after toggled selection showed induction by 14 mM adipic acid, with a maximum of 15.7-fold induction (Fig. 2B).

Next, qualitative differences in aTF regulatory mode-of-action suggest that inversion-of-function has occur in evolutionary history. For instance, PurR and TrpR act as repressors when in their ligand bound form<sup>37,38</sup>, LacI and TetR as repressors only in their apo-form<sup>39,40</sup>, while BenM acts as a co-activator when bound to CCM<sup>41</sup>. Indeed, previous directed evolution studies have demonstrated the identification of aTFs with reversed mode-of-action<sup>23-25,30</sup>. To probe the evolvability of BenM towards an inversion-of-function (i.e., deactivator/CCM as a co-repressor) using toggled selection following one round of directed evolution, we first sorted the aTF variant library for highly fluorescent variants in the absence of any ligand, indicative of auto-induction (OFF)(Fig. 2C). Next, we investigated 85 sorted clonal variants by flow cytometry in the presence and absence of inducer. From this screening we found three variants showing decreased reporter gene induction in the presence of CCM (ON). Because of the low success rate of 3.5% (3/85), we tested whether an additional round of sorting for cells that show low fluorescence in the presence of inducer would increase this fraction. From this second screen, we found that 185/285 (65%) after an additional round of negative selection in the presence of 5.6 mM CCM

224 showed a reduction in fluorescence, with one variant showing a 3.9-fold reduction in  
225 fluorescence. Overall, mean OFF state for first and second selection regimes were  
226  $1.3 \pm 0.7$  and  $0.6 \pm 0.3$ , respectively, while mean fold induction was  $2.5 \pm 1.3$  and  
227  $0.9 \pm 0.4$ , respectively, with the bulk of the second selection variants indeed being  
228 deactivated in the presence of CCM (Fig. 2C).

229 Lastly, a key parameter of biosensor performance is the operational range,  
230 i.e. the inducer concentration range in which the sensor shows a significant change  
231 in dose-responsive output. Since we found wild-type BenM to show significant  
232 induction by CCM from 0.56 mM CCM and upwards, we initially induced the BenM  
233 library with 0.035 or 0.070 mM CCM (Fig. 2D). Here, even though the uninduced and  
234 induced populations overlapped, we found that a gate based on the top-1% most  
235 fluorescent cells under induced conditions (ON) contained, when projected on the  
236 uninduced library (OFF), a smaller fraction of the population (i.e., 15% less for 0.035  
237 mM CCM and 20% less for 0.070 mM CCM)(Fig. 2D, Suppl. Table S1), suggesting  
238 the presence of variants induced by these low levels of CCM. Subsequent flow  
239 cytometry screening of sorted clonal variants showed that for both concentrations the  
240 mean OFF state was much lower ( $2.1 \pm 1.5$  for 0.035 mM CCM and  $1.6 \pm 1.0$  for  
241 0.07 mM CCM (Fig. 2D) than after a single round of positive selection for dynamic  
242 range and specificity variants (Fig. 2A-B). Therefore, a second round of sorting to  
243 remove auto-inducing variants was deemed unnecessary when evolving operational  
244 range variants. In addition, 16/95 (17%) variants for 0.035 mM and 55/95 (58%)  
245 variants for 0.070 mM CCM showed a notable fold-induction in the presence of  
246 ligand at the concentration they were sorted for (Fig. 2D).

247 In conclusion, FACS-driven selection regimes for all four parameters yielded  
248 new biosensor candidates for desired phenotypes. Toggled selection for dynamic  
249 range, affinity-maturation and inversion of function enabled a lowered mean OFF  
250 state compared to a single round of selection, whereas the operational range sorting  
251 strategy, by design, yielded low-OFF-state variants after a single round of selection.

252 Similarly, fold induction in ON states were higher following toggled selection  
253 compared to a single round of selection for dynamic and operational range variants,  
254 as well as for the affinity-matured BenM variants. Finally, for inversion-of-function  
255 variants toggled selection enabled identification of high OFF state variants with CCM-  
256 dependent transcriptional repression.

257

#### 258 *Transfer functions and mutation landscapes of evolved aTF variants*

259 To further characterize the evolved variants, sequencing and dose-response  
260 experiments of selected isoclonal BenM variants identified from the toggled selection  
261 regimes (Fig. 2A-D) were carried out.

262 By design, our pooled epPCR approach targeted 233 amino acids of BenM,  
263 which constitutes the 14-aa DBD-EDB linker, and the two EBD subdomains (I & II)  
264 held together by hinge-like  $\beta$ -strands resembling a periplasmic binding protein  
265 between which the ligand binds<sup>42</sup>. For the sequence-function analysis, we sequenced  
266 20 BenM mutants, of which three affinity-matured variants were identical. Sequence  
267 analysis of the 18 unique BenM variants covering the span of archetypical  
268 phenotypes (Fig. 2A-D) identified a total of 75 mutations across 58 positions in the  
269 233-aa window, with each BenM variant having between one (MP17\_F12) and six  
270 (DAP1\_H01) mutations (Fig. 3A-B) illustrative of the pooled epPCR approach  
271 undertaken. Moreover, one position (P201S) was mutated in all four specificity  
272 variants, two positions (T288I/S and Q291H) were mutated in three variants each,  
273 seven positions mutated in two variants each, and the remaining 48 positions  
274 mutated in only a single variant (Fig. 3A).

275 For dynamic range variants we carried out a dose-response characterization  
276 of three variants (Fig. 3B). Here we found that increased CCM induction was  
277 observed at all concentrations compared to WT BenM, and that the most highly-  
278 induced variant (MP2\_G10) displayed a dynamic range of 58.8  $\pm$  1.0, a more than  
279 15-fold improvement over BenM WT (Fig. 3C). Notably, different from other aTF

280 engineering efforts<sup>43</sup>, the increase in dynamic range was largely due to increased  
281 expression upon ligand induction, as only modest changes in OFF state expression  
282 was observed for the dynamic range variants compared to WT BenM (Fig. 2A).

283 For the operational range all seven titrated variants showed significant  
284 induction ( $p < 0.05$ ) at CCM concentrations below the lower detection limit of WT  
285 BenM (i.e. 0.56 mM CCM)(Fig. 3D). Specifically, MP17\_D08 significantly induced  
286 GFP expression from 0.014 mM CCM, a 40-fold improvement over WT BenM,  
287 whereas the remaining variants showed significant induction from 0.056 mM (Fig.  
288 3D). Interestingly, whereas most variants had shifted their operational range while  
289 maintaining a similar dynamic range as WT BenM, MP17\_D08 also displayed an  
290 increased dynamic range (Fig. 3D).

291 For the inversion-of-function variants, four variants were selected for dose-  
292 response analysis. Here, all variants showed dose-dependent deactivation for CCM  
293 (Fig. 3D), with one variant (MP05\_D07) showing similar fold-change (3.9-fold  
294 reduction) as WT BenM (5-fold induction) within the operational range of WT BenM,  
295 yielding a negative correlation coefficient of  $R^2 = -0.68$  compared to the transfer  
296 function of WT BenM (Fig. 3A and Fig. 3D).

297 Finally, for affinity-matured BenM variants, six mutants displayed >5-fold  
298 induction by adipic acid, of which three were sequence identical to variant MP04-  
299 B01. The response curve of the four unique variants was determined for adipic acid  
300 (Fig. 3E). One variant (TiSNO120) showed significant ( $p < 0.05$ ) induction from 1.4  
301 mM adipic acid, whereas the three other variants were significantly induced by 5.6  
302 mM adipic acid, whereas WT BenM was only induced from 14 mM ( $p = 0.03$ ; Fig.  
303 3B). With the exception of TiSNO120, the affinity-matured variants responded only  
304 modestly to CCM, corroborating the toggled selection regime (Suppl. Fig. S2, Fig.  
305 2B).

306 In summary, the toggled sorting scheme of a randomly mutated aTF EBD  
307 library serves as a powerful first demonstration of the impressive evolvability of

multiple aTF parameters from a single aTF platform, with aTF variants displaying up to 15-fold increased dynamic range, 40-fold change in operational range, new ligand-specificity, and inversion-of-function, compared to parental aTF.

311

### 312 *Structure-function relationships of evolved biosensor variants*

Interestingly, several of the amino acids mutated in this study (Fig. 3A) are known to affect BenM-dependent regulation of aromatic compound catabolism in native *Acinetobacter*<sup>44–46</sup>, revealing the structure-function relationships governing our observed phenotypes.

Furthermore, for dynamic range mutants, mutations exclusively occur in EBD-I, while operational range variants are the only ones with mutations occurring in the linker hinge between EDB-I and the DBD (Fig. 3A and 3F). The mutational space for aTF variants with inversion of function and matured affinities for adipic acid, on the other hand, all include broad mutation windows throughout both EBD subdomains (Fig. 3F).

In order to investigate more deeply the causality and mutational space involved in aTF variant calling, it is evident from our study, that single mutant E226V in variant MP17\_F12 is causal to aTF operational range. Additionally, while all specificity variants were different, they all shared the P201S mutation (Fig. 3A). Notably, residue 201 is involved in both binding of CCM and formation of the tetramer interface in BenM WT<sup>47</sup>, and in order to gain better understanding as to whether this residue is causal for changes in BenM ligand specificity, TiSNO120 (A130D, A153G, P201S, and E287V) was further investigated by analysing a series of single and combinatorial mutants introduced to WT BenM to evaluate their effects on biosensor read-out in response to 1.4 mM CCM or 14 mM AA (Suppl. Fig. S3). This confirmed the role of P201S in the increased response to adipic acid and decreased induction by CCM, although the re-introduction of a second mutation (E287V) was necessary to fully recapitulate the TiSNO120 phenotype.



336 Taken together, the sequencing and in-depth titration studies highlight  
337 regional mutational hotspots for the four different phenotypic categories of aTF  
338 variants, and further exemplifies the impact that single residue changes can have on  
339 aTF transfer function and specificity as exemplified by position E226 and P201 of  
340 BenM.

341

### 342 *Biochemical characterization of evolved aTF variants*

343 Small-molecule inducible transcription factors undergo interdomain DBD-EBD  
344 allosteric transitions upon DNA and ligand binding<sup>48</sup>. Also, HLH-type DBD of LTTRs  
345 bind DNA as dimers or tetramers, with BenM binding to the tripartite 73-nt binding  
346 site (*benO*) in the *ben* operon of *Acinetobacter sp. ADP1* as a tetramer<sup>49,50</sup>.  
347 Specifically, BenM functions as a dimer of dimers with deduced constitutive binding  
348 to dyad-symmetrical subsite 1 (ATAC-N7-GTAT), together with either subsite 2  
349 (ATAC-N7-GTGT) or subsite 3 (ATTC-N7-GTAT), in the presence or absence of  
350 CCM, respectively (Fig. 4A-B)<sup>50</sup>. Interestingly, and in line with the modular  
351 architecture of aTFs, Wang *et al.* have shown that substituting the cognate operator  
352 sequence with those of homologue aTFs can impact both dynamic and operational  
353 ranges of the biosensor<sup>51</sup>.

354 In order to determine if the transfer functions of aTF variants evolved from  
355 BenM EBD mutagenesis are coupled to changes in DNA-binding affinity, we  
356 performed biolayer interferometry (BLI). For this purpose, we heterologously  
357 expressed in *E. coli* and purified affinity-tagged WT BenM and archetypal variants  
358 from the four selection regimes (Fig. 2B-E) with homogenic purity and expected 43-  
359 44 kDa size ranges validated by SDS-PAGE<sup>50</sup>(Fig. 4C). Here, by titrating purified WT  
360 BenM (1.6-100 nM) onto immobilized *benO*, binding was observed, whereas no  
361 binding was observed to the negative control *cyc1* promoter element (Fig. 4D). This  
362 finding is in agreement with earlier *in vitro* studies of Bundy *et al.*<sup>50</sup>, and our earlier *in*  
363 *vivo* studies<sup>18</sup>. Next, performing BLI of all purified archetypal BenM variants, we

also observed DNA-binding affinity for *benO* (Fig. 4D). Interestingly, evolved archetypical BenM variants had similar equilibrium dissociation constant ( $K_D$ ) for *benO* (14.3 - 80 nM) as WT BenM (11.5 nM)(Fig. 4E). In addition to  $K_D$ 's, we calculated the Hill coefficient as described by Wang *et al.*<sup>52</sup>(see *Methods*) by plotting  $\log[\Theta/(1-\Theta)]$  as a function of the  $\log [\text{BenM}]$ (Fig. 4D-E, Suppl. Fig. S6). Moreover, in line with the biochemical and structural evidence of WT BenM, all of the evolved BenM variants maintained WT BenM's Hill coefficient of approx. 1, indicative of no cooperativity in DNA-binding (Fig. 4D-E, Suppl. Fig. S4).

Taken together, the low nM-range DNA-binding affinities observed across all archetypical BenM indicate that the evolved functionalities of the archetypal BenM variants are not due to secondary effects arising from perturbed DNA binding affinity, but rather a direct effect of EBD mutagenesis. Moreover, the elucidation of nearly identical protein structures of full-length WT BenM and two constitutively active BenM variants implies that even differences *in vivo* transcriptional activity are not well discriminated by structural studies<sup>46</sup>. Together these observations highlight that evolution-guided EBD designs offer a powerful method for engineering aTF functionalities, even dispensable of structural information.

381

### 382 *Portability of evolved biosensor variants into bacteria*

Prokaryote aTFs have been ported into eukaryotes for use as biosensors for decades<sup>53,54</sup>. In order to demonstrate the broader usefulness of high-throughput directed evolution of aTF-based biosensors evolved in yeast, we sought to demonstrate chassis portability. As an example biosensor we chose TiSNO120, a BenM variant affinity-matured for adipic acid biosensing - a molecule being one of the primary targets for platform chemicals in biorefineries<sup>55</sup>. As a recipient chassis we

389 choose *E. coli*, a commonly used biotechnology workhorse, with adipic acid tolerance  
390 up to 50 mM (Fig. 5A)<sup>56</sup>.

391 Transplanting the native BenM-binding (*benO*) bidirectional *Acinetobacter*  
392 promoter driving the expression of TiSNO120 and mCherry into *E. coli* resulted in  
393 TiSNO120-dependent expression of mCherry within the 0-35 mM adipic acid range  
394 (Fig. 5B), exemplifying the robustness and broader usefulness of high-throughput  
395 biosensor prototyping in yeast.

396

## 397 Discussion

398 In the present study, directed evolution coupled with toggled selection  
399 regimes was used to successfully identify novel aTF variants with user-defined  
400 transfer functions and change of specificity. To the best of our knowledge, the  
401 toggled sorting scheme of a randomly mutated aTF EBD served as a powerful first  
402 demonstration of the evolvability of multiple aTF parameters from a single aTF  
403 platform. Moreover, this study demonstrate yeast as a robust model chassis for  
404 prokaryote biosensor prototyping, and that the high-throughput workflow outlined in  
405 this study not only arms synthetic biologists with new biosensors, but also enables  
406 broader host-agnostic usability, as exemplified by the adipic acid biosensor variant  
407 being functional in *E. coli*. Finally, in this study, the starting point was BenM from  
408 *Acinetobacter sp. ADP1*, a natively CCM-inducible transcription factor, which belongs  
409 to the largest family of prokaryotic aTFs, namely LTTRs, which could as such serve  
410 as platform aTFs for further expanding the functional space of many new-to-nature  
411 biosensors.

412 Another important observation is the similar DNA-binding affinities broadly  
413 observed for all four classes of aTF variants (Fig. 4). For operational range variants,  
414 this indicates that beyond the strategy of using degenerate or multi-copy operator  
415 sequences to change biosensor operational ranges<sup>51</sup>, engineering aTFs by EBD  
416 mutagenesis is a new route to change biosensor operational range. Beyond the

operational range mutants, the DNA binding affinity of inversion of function variants is particularly alluring. Given WT-like DNA binding affinity, several hypotheses on the molecular mechanisms can explain the ligand-dependent repression. Firstly, it could be speculated that the variant aTF represses rather than activates transcription by binding elsewhere in the reporter promoter, or that the mutant has increased ligand-independent DNA affinity. However, as no mutations were targeted in the DBD region of BenM, and that the BenM variants are able to bind the cognate operon for wild-type BenM with similar  $K_D$  (Fig. 4), both of these scenarios are considered unlikely. More likely, given the occurrence of five mutations in variant MP05\_D07 (E137D, V166I, E277D, Q291H, and G297R), we hypothesize that the inversion could be related to a modification of the allosteric transition itself. In this scenario, the evolved BenM would not bind the operator with CCM bound. Instead, the variants would have a high affinity, yet be in allosteric ON state, for the *benO* operator in the absence of CCM, analogously to the mechanism hypothesized for anti-LacI variants<sup>30</sup>. In addition, R225H is known to cause high OFF-state and decreased dynamic range<sup>45</sup>, potentially adding to the full inversion of function of variant P2\_H02 containing mutation R225K in addition to four other mutations.

Although the phenotypic screen developed in this study proved useful for generating aTF variants with user-defined performance parameters, complementing biochemical characterization has also proven effective for understanding structural and mechanistic differences of mutant aTFs<sup>57</sup>. Since a change in phenotype can occur due to one or any combination of (i) altered specificity and/or affinity for an inducer, (ii) expression levels and protein stability, (iii) DNA binding affinity, and (iv) presence of protein subunits in active or inactive conformations, the more detailed mechanistic effects should be investigated for purified aTF variants from different phenotypic categories<sup>57</sup>. For instance, for any oligomeric DNA-binding aTF, it will be relevant to analyze the oligomerization state and molecular dynamics, as well as ligand affinity to determine how each of these functions could affect aTF variant

performance, and thus improve our understanding of how individual or combinations of mutations affect aTF structure and function, and thereby enable more rational biosensor engineering.

Ultimately, combining the functional and high-throughput evolution-guided method presented in this study, together with computational design of ligand binding and structural dynamics, should enable a multi-faceted approach, necessary to gain better understanding of biosensor allostery, and how this can be forward-engineered for future designer biosensors.

## Methods

### *Medium and chemicals*

Stable *S. cerevisiae* strains were routinely cultivated at 30 °C on YPD (1% (w/v) yeast extract, 2% (w/v) peptone 2% (w/v) dextrose, solidified with 2% (w/v) agar) medium, whereas plasmid-containing strains or libraries were cultivated in synthetic complete medium lacking leucine (SC-Leu; 6.7 g/L yeast nitrogen base without amino acids, 1.62 g/L yeast synthetic drop-out medium supplement without leucine (Y1376, Sigma-Aldrich), 2% (w/v) dextrose, pH 5.6, 2% (w/v) agar in case of plates). Mineral medium supplemented with tryptophan (7.5 g/L (NH<sub>4</sub>)<sub>2</sub>SO<sub>4</sub>, 14.4 g/L KH<sub>2</sub>PO<sub>4</sub>, 0.5 g/L MgSO<sub>4</sub>•7H<sub>2</sub>O, 2 g/L dextrose, trace metals, vitamins, 0.02 g/L tryptophan, pH 4.5) was freshly prepared as described previously<sup>58</sup>, and medium was handled as outlined by Ambri *et al.*<sup>59</sup>. Diacids, *cis*, *cis*-muconic acid (Sigma, CAS Number 1119-72-8, Product Number: 15992) or adipic acid (TCI, CAS Number:124-04-9 Product Number: A0161), were dissolved freshly to the medium on the day of handling, after which the pH was adjusted to 4.5 and the solution filter-sterilized as previously described<sup>59</sup>.

EasyClone plasmids used in this paper are outlined in Jensen *et al.*<sup>58</sup>. *Escherichia coli* strain DH5 was used as a host for cloning and plasmid propagation,

473 and cultivated at 37 °C in Luria-Bertani (LB) medium supplemented with 100 ug/mL  
474 ampicillin. PCR was carried out using Phusion® or Phusion U High-Fidelity DNA  
475 Polymerase (New England Biolabs) according manufacturer's instructions. Site-  
476 directed mutagenesis of BenM in pMeLS0076 was carried out using the QuikChange  
477 Site-Directed Mutagenesis Kit (Agilent Technologies) according to manufacturer's  
478 instructions.

479 Yeast transformation was performed according to Gietz & Schiestl<sup>60</sup>, followed  
480 by selection on synthetic drop-out medium.

481 All oligonucleotides, plasmids, strains, and synthetic DNA used in this study  
482 are listed in Suppl. Table S2.

483

#### 484 *Library generation*

485 In order to generate a library of mutated fragments of the BenM-EBD the  
486 procedure described by Skjoedt *et al.*<sup>18</sup> was followed. In short, epPCR was carried  
487 out using the Agilent GeneMorph mutagenesis II kit following manufacturer's  
488 instructions for high mutational load. Five consecutive rounds of epPCR were carried  
489 out using primers MeIS69-F and MeIS93-R, using 50 ng pMeIS0076 as a starting  
490 template for the first round of PCR. After each round, the 735-bp band was gel-  
491 purified, and 50 ng was used as input for the next round. To make a library of yeast  
492 strains, mutated fragments from rounds 2-5 were used as input for four regular PCRs  
493 (Phusion) using tailed primers MeIS071-F and MeIS094-R and column-purified.  
494 Pooled fragments from rounds 2 and 3 (sublibrary 1), as well as rounds 4 and 5  
495 (sublibrary 2), were co-transformed with gapped vector pMeIS0076 into strain  
496 MeIS009 (CEN.PK with chromosomal integration of yeGFP reporter gene) in a molar  
497 ratio of 80:1, in order to allow for re-constitution of the plasmid. For each sublibrary  
498 two transformations were carried out ( $4 \times 10^7$  cells as input each), the total biomass  
499 was pooled afterwards, added to 48 mL SC-leu, grown overnight to saturation and  
500 frozen in aliquots (sublibrary 1, TISNO-122; sublibrary 2, TISNO-123). From plating

for single colonies right after transformation it was found that sublibrary 1 contained 224,000 variants, and sublibrary 2 contained 198,000 variants. Colony PCR and sequencing of 10 random colonies per sublibrary narrowed down the library size for sublibrary 1 to 45,000 effective variants, and sublibrary 2 to 40,000 effective variants. In this article sublibrary 1 and 2 are always combined for sorting purposes (effectively containing 85 000 variants) and referred to as 'the BenM library'.

507

#### 508 *FACS-based selection*

For all sorting steps *S. cerevisiae* cells containing the BenM library or subpopulations thereof previously frozen in 25% (v/v) glycerol at -80 °C were thawed and added to 5 mL SC-Leu to become OD<sub>600</sub> = 0.2 (approx. 2 x 10<sup>6</sup> cells/mL). Cultures were grown overnight in 12-mL preculture tubes in a 30 °C incubator shaking at 300 rpm with 5 cm orbit diameter. The next day, cultures were diluted into minimal medium +/- inducer to OD<sub>600</sub>=0.2 and incubated under the same conditions. In parallel, control strains were processed similarly. After 22 h each culture was diluted in 2 mL sterile 1x PBS to an OD<sub>600</sub> of approx. 1.0 right before being analyzed on a Becton Dickinson Aria fluorescence-assisted cell sorting (FACS) instrument with a blue laser (488 nm) to detect yeGFP fluorescence. For control strains 10,000 single-cell events were measured and for (sub)libraries 250,000 events were measured to assess mean fluorescence intensity and diversity of each population in medium with or without inducer. Depending on the phenotype under study, specific gates were drawn to select for single-cell events obeying the set criterion (Fig. S2). In any case, cells were sorted in FITC-A vs FSC-A plot in order to select based on fluorescence intensity without bias for a certain cell size as carried out previously<sup>61,62</sup>. Sorted cells were collected in 2-5 mL SC-Leu (initial cell density < 5,000 cells/ mL) and allowed to recover overnight (30 °C, 300 rpm) until a sufficient OD<sub>600</sub> was reached after which cells were frozen down in 25% (v/v) glycerol at -80 °C in aliquots containing 2.5 OD<sub>600</sub> units each.

529

# 530 *Flow cytometry*

531 Flow cytometry screening was carried out as described previously<sup>18</sup>. In short,  
532 clonal variants were inoculated into 150 µL SC-Leu in 96-well plates and grown  
533 overnight. The next day, strains were subcultured 1:100 into 500 µL medium +/-  
534 inducer in a deep-well plate and cultured for 22-23 h before analyzed by flow  
535 cytometry. In parallel, control strains ST.1 (WT CEN.PK), MeLS0138 (reporter-only)  
536 and MeLS0275 (BenM WT – reporter) were processed in the same fashion in  
537 biological triplicates in each experiment. The mean fluorescence intensity (MFI) of  
538 each strain was determined based on 10 000 gated single-cell events. The  
539 normalized OFF state of each variant was determined by dividing its MFI in control  
540 medium by the average MFI of MeLS0275 in control medium in the same  
541 experiment.

542

# 543 *Protein expression and purification*

544 BenM and its variants were expressed in *E. coli* BL21 (DE3). An overnight  
545 culture grown in 2xYT was used to inoculate 0.5 L MagicMedia (Invitrogen), both  
546 supplemented with 50 µg/mL kanamycin, grown at 37 °C and shaking at 200 rpm.  
547 When the OD<sub>600</sub> reached 0.6, cells were transferred to 18 °C and incubated for 36  
548 hours. After harvest, cells were lysed by three passes through an emulsiflex C5  
549 (Avestin, Mannheim, Germany) and cleared cell lysate was loaded onto a HisTrap FF  
550 column (GE Healthcare). After washing with 10 column volumes of buffer A (30 mM  
551 Tris-HCl, 500 mM NaCl, 30% Glycerol, 5 mM Imidazole, 1 mM DTT pH 7.9), proteins  
552 were eluted with 4 column volumes each of 5%, 10%, 15% and 100% buffer B (30  
553 mM Tris-HCl, 500 mM NaCl, 30% Glycerol, 500 mM Imidazole, 1 mM DTT pH 7.9).  
554 When purity was unsatisfactory, protein were polished on a HiLoad 16/600 Superdex  
555 200pg column equilibrated in 50 mM Tris-HCl, 150 mM NaCl pH 8.0. Proteins were  
556 frozen in N<sub>2</sub>(l) and stored at -80 °C.



557

## 558 *Biolayer interferometry*

559 Synthetic 5'-end biotinylated (forward) and non-modified (reverse) single-  
560 stranded DNA oligos were ordered from IDT (Integrated DNA Technologies,  
561 Coralville, IA), and resuspended to final concentrations of 200 nM in IDT Nuclease-  
562 free duplex buffer according to manufacturer's instructions. Complementary single-  
563 stranded oligos for preparing 209bp\_CYC1p (TISNO-110 and TISNO-113) and  
564 209bp\_*benO*\_CYC1p (TISNO-112 and TISNO-114) were combined in 1:1 ratios  
565 using 20 uL of each oligo, and incubated at 94 °C for 2 min. Next the mixtures were  
566 left at RT for 3 hrs before storing them as 2.5 uL aliquots of 100 μM DNA (0.25  
567 mol/aliquot). Using 0.2 nmol of DNA for each experiment, all DNA binding  
568 experiments were performed using an FortéBio Octet RED96 (Pall, Menlo Park, CA,  
569 USA) mounted with black 96-well microplates at 30 °C with 200 μL volume.  
570 Streptavidin sensors (Pall, Menlo Park, CA, USA) were pre-equilibrated in PBS buffer  
571 for 600s and loaded with biotinylated 209bp\_CYC1pro or 209bp\_*benO*\_CYC1pro  
572 (100 nM, 600s). After reaching baseline for 300s, association and dissociation of the  
573 indicated concentrations of BenM WT and variants were measured for 600s each. All  
574 assay steps were performed in kinetics buffer (PBS containing 0.02% Tween-20 v/v  
575 and 0.1% BSA w/v, pH 7.4). Binding kinetics were calculated using the FortéBio Data  
576 Analysis v7.1 software by fitting the association and dissociation data to a 1:1 model.  
577 A cut-off of  $R^2 > 0.95$  was used in order to ensure binding kinetics were calculated  
578 only when there was a good fit between calculated and measured binding curves.

579 The measured signal at equilibrium, noted  $R_{eq}$ , and the calculated  $R_{max}$  for  
580 each protein concentration were used to calculate fractional saturation and plotted  
581 against the respective protein concentration to determine the Hill coefficient  
582 according to Engohang-Ndong *et al.*<sup>63</sup>

583

584 
$$\text{Fractional saturation} = \square = R_{eq}/R_{max}$$

$$X = \log[\text{BenM-His}]$$

$$Y = \log(\square/(1-\square))$$

587

# 588 *Analysis of BenM variants by sequencing*

589 Fold-change (FC) fluorescence induction was calculated for each data point  
590 comparing the fluorescence level in the control medium and the fluorescence level in  
591 the inducer media. The displayed score for the phenotypes of improved dynamic and  
592 operational range, as well as for change of specificity, were computed normalising  
593 the mutants' FC values by the FC value of the wild type protein at the same  
594 conditions. The Pearson correlation coefficient (PCC) was calculated using FC  
595 values of the mutated phenotype and FC values of the wild type phenotype at  
596 increasing concentrations. The dynamic ranges were calculated for the wild type  
597 ( $R_{wt}$ ) and for the mutant ( $R_v$ ) phenotypes, as the difference between the  
598 corresponding highest and lower values of FC:

599

$$R_{wt} = (FC_{\text{highest}} - FC_{\text{lowest}})$$

$$R_v = (FC_{\text{highest}} - FC_{\text{lowest}})$$

602

603 Additionally, the ratio between  $R_v$  and  $R_{wt}$  was used as coefficient to indicate  
604 the similarity of dynamic range between the mutant and the wild type. The inversion  
605 of function phenotype score (X) was calculated multiplying the PCC and the ratio  
606 between  $R_v$  and  $R_{wt}$ :

607

$$X = \text{PCC}_{v\_vs\_wt} * (R_v / R_{wt})$$

609

610 Where the highest inversion of function corresponds to high anti-correlation (PCC ~ -  
611 1) and similar dynamic range ( $R_v / R_{wt} \sim 1$ ).

612

# 613    *Biosensing in E. coli*

614            The adipic acid biosensing plasmid (JBx\_101898) was assembled of 4 DNA  
615 parts by NEBuilder® HiFi DNA Assembly Master Mix (New England Biolabs, MA):  
616 First, the 3.3 kb backbone was amplified from pBbS5c-RFP (JBp\_000017) using  
617 primers                    j5\_00193\_(pBbS5c\_backbone)\_forward                    and  
618 j5\_00194\_(pBbS5c\_backbone)\_reverse. Next, the 0.9 kb *benM\_Mu1* was amplified  
619 from pTS-56 using primers j5\_00195\_(BenM\_Mu\_rc)\_forward and  
620 j5\_00196\_(BenM\_Mu\_rc)\_reverse, while BP-01, the 0.3 kb DNA binding site of  
621 BenM (*benO*) with overlap regions, was synthesized as gBlocks® Gene Fragment  
622 (Integrated DNA Technologies, Inc., IA). Lastly, the 0.7 kb *mCherry* was amplified  
623 from pSC-gapdhp(EL)-mCherry (JBx\_065530) using primers  
624 j5\_00198\_(mCherry)\_forward and j5\_00199\_(mCherry)\_reverse. The negative  
625 control plasmid (JBx\_101899) was constructed via self-circularization: primers  
626 BenM\_KO\_R and BenM\_KO\_F were used to amplify the 4.3 kb fragment from  
627 JBx\_101898, the PCR product was self-circularized by T4 ligase (Thermo Fisher  
628 Scientific Inc., MA).

629            The *E. coli* DH10B transformed with JBx\_101898 (JBx\_101900) was used for  
630 adipic acid biosensing, while the *E. coli* DH10B transformed with JBx\_101899  
631 (JBx\_101901) was used as negative control. The *E. coli* cell was grown overnight in  
632 Luria–Bertani (LB) medium containing 25 µg/mL chloramphenicol at 37 °C. The  
633 overnight culture was inoculated 1:100 at 50 mL fresh LB medium containing  
634 chloramphenicol and grown at 37 °C. Once the OD600 reached 0.6, the culture was  
635 cooled down to room temperature and aliquoted into 96-well deep well plate (2 mL  
636 volume, V-bottom) at 0.5 mL per well. The adipic acid aqueous stock was prepared  
637 at 1.7 M with pH = 7.0 (adjusted by NaOH) and filtered with 0.22 µm filter. The  
638 working solutions with varying concentrations were diluted with sterile water from the

639 stock. 10  $\mu$ L of working solution was added to each well to make the adipic acid final  
640 concentrations (mM) at 0, 0.02, 0.05, 0.1, 0.2, 0.5, 1, 2, 4, 8, 16, 32. The deep well  
641 plate was sealed by AeraSeal film (Omega Bio-tek, Inc., GA) and wrapped by  
642 aluminum foil. The plate was shaken at 250 rpm in 30 °C for 16 h. After that, 100  $\mu$ L  
643 culture from each well was transferred into 96-well Costar® assay plate (black with  
644 clear flat bottom, Corning Inc., NY) to measure the optical density at the wavelength  
645 of 600 nm absorbance and mCherry fluorescence ( $\lambda_{ex}$  = 575 nm,  $\lambda_{em}$  = 620 nm,  
646  $\lambda_{cutoff}$  = 610 nm) by SpectraMax M2 plate reader (Molecular Devices, LLC., CA).  
647 The assays were performed in triplicate wells for each concentration.

648

## 649 **Acknowledgements**

650 This work was supported by the Novo Nordisk Foundation.

651

## 652 **Author contributions**

653 T.S., E.K.C., J.D.K., and M.K.J. conceived this project. T.S., E.K.C., B.P., J.F.B., S.  
654 P.B., and S.K. designed all of the experiments. F.A., E.K.C., and D.H.W performed  
655 all structure-function analysis. T.S., E.K.C., B.P., J.F.B., S. P.B., S.K. and M.K.J  
656 analyzed the data. T.S. and M.K.J. wrote the paper.

657

## 658 **Conflicts of interest**

659 J.D.K. has a financial interest in Amyris, Lygos, Demetrix, Constructive Biology,  
660 Maple Bio, and Napigen.

661

## 662 **Figure legends**

663

664 **Fig. 1. Schematic outline of directed evolution of aTF transfer functions and**  
665 **specificities. (A)** Overview of experimental workflow using a single round of directed  
666 evolution followed by *in vivo* gap repair of aTF variant library in yeast, and finally

667 toggled FACS-based selection of desired transfer function parameters. Protein  
668 structure depicts monomeric BenM (PDB 3k1n). (B) Illustration of a wild-type aTF  
669 transfer function (black) and evolved transfer functions (red) for the traits of interest,  
670 namely operational range, dynamic range, and inversion of function, as well as  
671 ligand-specificity.

672

673 **Fig. 2. Directed evolution of aTF transfer functions and specificities.** *Leftmost*

674 *and middle-left panels:* Representative flow cytometry green fluorescence protein  
675 (GFP) intensity distributions showing the yeast library, or sublibraries thereof,  
676 expressing BenM-EBD variants in control (OFF) or inducer medium (ON) and/or a  
677 strain not expressing BenM in control medium (No BenM), and dashed lines  
678 indicating the sorting gate. (A-B) *Leftmost and middle-left panels:* Toggled selection  
679 for dynamic range (A) or affinity maturation (B). In the first round of selection cells  
680 were sorted from the yeast library induced with 1.4 mM CCM (A) or 14 mM adipic  
681 acid (B) showing higher fluorescence than the uninduced library. In the second round  
682 of selection only variants from the uninduced population were sorted showing  
683 background fluorescence, based on a strain not expressing BenM in control medium.

684 *Middle-right panels:* Toggled selection of variants with increased dynamic  
685 range in response to CCM (A) and adipic acid (B) show reduced mean OFF state  
686 compared to a single round of ON selection. Dashed blue indicate BenM WT OFF  
687 state. *Right panels:* Toggled selection of variants with increased dynamic range in  
688 response to CCM (A) or change in ligand-specificity (B) towards adipic acid show  
689 increased mean fold-induction compared to a single round of ON selection. Dashed  
690 blue indicate BenM WT ON state for CCM (2.8x) or adipic acid (1.1x). (C) *Leftmost*  
691 *and middle-left panel:* Toggled selection for inversion of function. In the first round of  
692 selection cells were sorted from the uninduced yeast library showing higher  
693 fluorescence than a strain not expressing BenM in control medium. In the second  
694 round of selection only variants from the population induced with 5.6 mM CCM were

sorted showing higher than background fluorescence, based on a strain not expressing BenM in control medium. *Middle-right panel:* Toggled selection of clonal variants with inversion of function phenotype show reduced mean OFF state compared to a single round of ON selection. Dashed blue indicate BenM WT OFF state. *Right panel:* Toggled selection of variants with inversion of function phenotype in response to CCM show decreased mean fold-induction compared to a single round of ON selection. Dashed blue indicate a fold-induction of 1.0. **(D)** *Leftmost panels:* Selection for operational range. Cells were sorted from the yeast library induced with 0.035 mM CCM (Selection I) or 0.070 mM CCM (Selection II) showing higher fluorescence than the uninduced library. *Middle-right panel:* Clonal variants gated from inducer media with changed operational range show lowered mean OFF state compared to a single round of positive selection for variants in (A-B). Dashed blue indicate BenM WT OFF state. *Right panel:* Fold-change of variants with changed operational range in response to either 0,035 or 0,07 mM CCM. Dashed blue line indicates fold-induction of WT BenM at the two concentrations (0.90 +/- 0.05 and 1.02 +/- 0.14 for 0.035 mM CCM and 0.070 mM CCM, respectively).

711

**Fig. 3. Sequence-function characterization of BenM WT and evolved archetypical variants.** **(A)** Amino-acid substitution profiles for the four phenotypic categories (*Left*) of evolved BenM variants, with heat-mapping to indicate the BenM variant fold-induction for the lowest inducer concentration with a significant ( $p < 0.05$ ) response compared to control medium. The displayed score (*Right*) for the archetypical variants of improved dynamic and operational range, as well as for change of specificity, is indicative of fold-change between inducer and control medium for the lowest inducer concentration significantly improving ON state compared to OFF state as indicated in *Methods*. For the inversion-of-function variants, the score represents the correlation coefficient between dose-response curves for WT BenM and evolved variants calculated according to equation given

723 *Methods.* **(B)** Depictions of BenM monomeric structures (PDB 3k1n), with domains  
724 color-coded for mutational spaces for each of the four phenotypic categories. **(C-F)**  
725 Dose-response curves for BenM variants, BenM WT, and reporter-only control (No  
726 BenM). Data represents mean fold induction for dynamic range (C), operational  
727 range (D) affinity-matured (E), and fluorescence intensities for inversion-of-function  
728 variants operational range variants (F), +/- SD from three biological replicates. a.u. =  
729 arbitrary units.

730

731 **Fig. 4. Biochemical characterization of BenM WT and evolved archetypical**

732 **variants.** **(A)** Tetrameric representation of full-length BenM (PDB: 3K1N)  
733 superimposed on BenM-DBD-DNA complex (PDB:4IHT)<sup>46</sup>. The dimeric structure of  
734 full-length BenM (PDB: 3K1N) was used to generate the probable tetrameric  
735 assembly using PDBePISA<sup>64</sup> and bioassembly 1 was chosen due to the higher  $\Delta G^{diss}$   
736 when compared to the alternative tetrameric bioassembly 2. The BenM-DBD-DNA  
737 complex (PDB:4IHT) was superimposed on the tetrameric assembly using PyMOL.  
738 **(B)** The sequence outline of DNA fragments 209bp\_CYC1pro and  
739 209bp\_benO\_CYC1pro, with BenM binding sites, according to Bundy *et al.*<sup>50</sup>,  
740 highlighted in bold red. **(C)** Expression of His<sub>6</sub>-tagged BenM wild type (WT) and nine  
741 archetypal variants in *E. coli* (BL21). Following batch affinity purification, the eluents  
742 from WT BenM and BenM variants were visualized on SDS/PAGE by Coomassie  
743 blue staining. Arrow indicate expected size of purified proteins. **(D)** Interaction  
744 between WT BenM WT and DNA fragments 209bp\_CYC1pro and  
745 209bp\_benO\_CYC1pro measured using biolayer interferometry (BLI) for real-time  
746 analysis of interactions between fragments 209bp\_CYC1pro and  
747 209bp\_benO\_CYC1pro and increasing concentrations of BenM WT (1.56, 3.13, 6.25,  
748 12.5, 25, 50 and 100 nM). Following initial loading of 100 nM biotinylated fragments  
749 209bp\_CYC1pro or 209bp\_benO\_CYC1 onto streptavidin tips, 600 sec of  
750 association and dissociation of BenM was performed (see *Methods*). The BLI signals

751 for association at titrated BenM WT concentrations and dissociation, and the  
752 calculated  $K_d$ 's are shown. (E) Determination of binding affinity between *benO* and  
753 BenM variants by BLI. As for (C) the BLI signals for association at 100 nM BenM  
754 variant concentrations and dissociation, and the calculated  $K_d$ 's are shown. Dashed  
755 red line in (C-D) mark the fitting of the experimental association and dissociation data  
756 to a 1:1 model, with a cut-off of  $R^2 > 0.95$  of between calculated and measured  
757 binding curves for calculating binding kinetics. n.d. = not determined.

758

759 **Fig. 5. Host portability of evolved atF biosensors variants.** (A) Schematic outline  
760 of biosensor prototyping on different chassis. (B) Dose-response curves for BenM  
761 variant TISNO-120 (BenM\_TISNO120) affinity.-matured for adipic acid biosensing vs  
762 no BenM expression (reporter-only) in *E. coli*. Data represents mean fluorescence  
763 intensities for mCherry/OD +/- SD from three biological replicates. a.u. = arbitrary  
764 units.

765

766 **Supplementary material**

767

768 **Supplementary Fig. S1. Multiple sequence alignment of the protein sequences**  
769 **of 12 LTTRs.** Alignment, including WT BenM and other yeast-implemented LTTRs  
770 FdeR, ArgP, MdcR and PcaQ, was generated using T-Coffee and visualized using  
771 Boxshade<sup>65</sup>. Fraction cut-off for sequence shading was set at 0.7.

772

773 **Supplementary Fig. S2. CCM-responsiveness of adipic acid affinity-matured**  
774 **BenM variants.** Measurements are means +/- SEM from three independent  
775 biological replicates. a.u. = arbitrary units.

776

777 **Supplementary Fig. S3. Effects of single and double mutations in biosensor**  
778 **performance.** Individual and combinations of mutations found in BenM variant



779 TiSNO120 were introduced to WT BenM, and transformed into a reporter strain  
780 expressing GFP under the control of the truncated synthetic 209\_CYC1\_*benO*  
781 promoter in yeast. CCM = *cis,cis*-muconic acid. AA = Adipic acid. a.u. = arbitrary  
782 units.

783

784 **Supplementary Fig. S4. Hill plot for WT BenM and BenM variants binding to**  
785 **DNA fragment *benO*.** The equation is indicated for each protein and the slope of  
786 0.99-1.00 corresponds to the Hill coefficient. Req was measured and Rmax was  
787 calculated independently for each protein concentration. The calculations were  
788 performed as previously described<sup>63</sup>.

789

790 **Supplementary Table S1.** Overview of FACS regimes for evolution-guided aTF  
791 transfer function engineering and affinity-maturation.

792

793 **Supplementary Table S2.** Overview of strain, plasmids, primers, and gBlocks used  
794 in this study.

795

## 796 **References**

- 797 1. Lutz, R. & Bujard, H. Independent and tight regulation of transcriptional units in  
798 *Escherichia coli* via the LacR/O, the TetR/O and AraC/I1-I2 regulatory elements.  
799 *Nucleic Acids Res.* **25**, 1203–1210 (1997).
- 800 2. Raman, S., Rogers, J. K., Taylor, N. D. & Church, G. M. Evolution-guided  
801 optimization of biosynthetic pathways. *Proceedings of the National Academy of*  
802 *Sciences* **111**, 201409523 (2014).
- 803 3. Kotula, J. W. *et al.* Programmable bacteria detect and record an environmental  
804 signal in the mammalian gut. *Proc. Natl. Acad. Sci. U. S. A.* **111**, 4838–4843  
805 (2014).

- 806 4. Galloway, K. E., Franco, E. & Smolke, C. D. Dynamically reshaping signaling  
807 networks to program cell fate via genetic controllers. *Science* **341**, 1235005  
808 (2013).
- 809 5. Chen, Y., Kim, J. K., Hirning, A. J., Josi, K. & Bennett, M. R. Emergent genetic  
810 oscillations in a synthetic microbial consortium. *Science* **349**, 986–989 (2015).
- 811 6. Finn, R. D. *et al.* InterPro in 2017-beyond protein family and domain annotations.  
812 *Nucleic Acids Res.* **45**, D190–D199 (2017).
- 813 7. Lin, J.-L., Wagner, J. M. & Alper, H. S. Enabling tools for high-throughput  
814 detection of metabolites: Metabolic engineering and directed evolution  
815 applications. *Biotechnol. Adv.* **35**, 950–970 (2017).
- 816 8. Werten, S., Schneider, J., Palm, G. J. & Hinrichs, W. Modular organisation of  
817 inducer recognition and allostery in the tetracycline repressor. *FEBS J.* **283**,  
818 2102–2114 (2016).
- 819 9. Delépine, B., Libis, V., Carbonell, P. & Faulon, J.-L. SensiPath: computer-aided  
820 design of sensing-enabling metabolic pathways. *Nucleic Acids Res.* **44**, W226–  
821 31 (2016).
- 822 10. Stanton, B. C. *et al.* Genomic mining of prokaryotic repressors for orthogonal  
823 logic gates. *Nat. Chem. Biol.* **10**, 99–105 (2013).
- 824 11. Shis, D. L., Hussain, F., Meinhardt, S., Swint-Kruse, L. & Bennett, M. R.  
825 Modular, multi-input transcriptional logic gating with orthogonal LacI/GalR family  
826 chimeras. *ACS Synth. Biol.* **3**, 645–651 (2014).
- 827 12. Juárez, J. F., Lecube-Azpeitia, B., Brown, S. L., Johnston, C. D. & Church, G. M.  
828 Biosensor libraries harness large classes of binding domains for construction of  
829 allosteric transcriptional regulators. *Nat. Commun.* **9**, 3101 (2018).
- 830 13. De Paepe, B., Maertens, J., Vanholme, B. & De Mey, M. Chimeric LysR-type  
831 transcriptional biosensors for customising ligand specificity profiles towards  
832 flavonoids. *ACS Synth. Biol.* (2018). doi:10.1021/acssynbio.8b00326
- 833 14. Feng, J. *et al.* A general strategy to construct small molecule biosensors in

- 834 eukaryotes. *Elife* **4**, (2015).
- 835 15. Banaszynski, L. A., Chen, L.-C., Maynard-Smith, L. A., Ooi, A. G. L. &  
836 Wandless, T. J. A rapid, reversible, and tunable method to regulate protein  
837 function in living cells using synthetic small molecules. *Cell* **126**, 995–1004  
838 (2006).
- 839 16. Brandsen, B. M., Mattheisen, J., Noel, T. & Fields, S. A biosensor strategy for E.  
840 coli based on ligand-dependent stabilization. *ACS Synth. Biol.* (2018).  
841 doi:10.1021/acssynbio.8b00052
- 842 17. Meinhardt, S. *et al.* Novel insights from hybrid LacI/GalR proteins: family-wide  
843 functional attributes and biologically significant variation in transcription  
844 repression. *Nucleic Acids Res.* **40**, 11139–11154 (2012).
- 845 18. Skjoedt, M. L. *et al.* Engineering prokaryotic transcriptional activators as  
846 metabolite biosensors in yeast. *Nat. Chem. Biol.* **12**, 951–958 (2016).
- 847 19. Xiong, D. *et al.* Improving key enzyme activity in phenylpropanoid pathway with  
848 a designed biosensor. *Metab. Eng.* **40**, 115–123 (2017).
- 849 20. Marvin, J. S. *et al.* The rational design of allosteric interactions in a monomeric  
850 protein and its applications to the construction of biosensors. *Proc. Natl. Acad.*  
851 *Sci. U. S. A.* **94**, 4366–4371 (1997).
- 852 21. Taylor, N. D. *et al.* Engineering an allosteric transcription factor to respond to  
853 new ligands. *Nat. Methods* **13**, 177–183 (2015).
- 854 22. Meyer, S. *et al.* Engineering alternate cooperative-communications in the lactose  
855 repressor protein scaffold. *Protein Eng. Des. Sel.* **26**, 433–443 (2013).
- 856 23. Richards, D. H., Meyer, S. & Wilson, C. J. Fourteen Ways to Reroute  
857 Cooperative Communication in the Lactose Repressor: Engineering Regulatory  
858 Proteins with Alternate Repressive Functions. *ACS Synth. Biol.* **6**, 6–12 (2017).
- 859 24. Ike, K. *et al.* Evolutionary Design of Choline-Inducible and -Repressible T7-  
860 Based Induction Systems. *ACS Synth. Biol.* **4**, 1352–1360 (2015).
- 861 25. Scholz, O. *et al.* Activity reversal of Tet repressor caused by single amino acid

- 862 exchanges. *Mol. Microbiol.* **53**, 777–789 (2004).
- 863 26. Suckow, J. *et al.* Genetic studies of the Lac repressor. XV: 4000 single amino  
864 acid substitutions and analysis of the resulting phenotypes on the basis of the  
865 protein structure. *J. Mol. Biol.* **261**, 509–523 (1996).
- 866 27. Tang, S.-Y., Fazelinia, H. & Cirino, P. C. AraC regulatory protein mutants with  
867 altered effector specificity. *J. Am. Chem. Soc.* **130**, 5267–5271 (2008).
- 868 28. Collins, C. H., Leadbetter, J. R. & Arnold, F. H. Dual selection enhances the  
869 signaling specificity of a variant of the quorum-sensing transcriptional activator  
870 LuxR. *Nat. Biotechnol.* **24**, 708–712 (2006).
- 871 29. Meyer, A. J., Segall-Shapiro, T. H., Glassey, E., Zhang, J. & Voigt, C. A.  
872 Escherichia coli ‘Marionette’ strains with 12 highly optimized small-molecule  
873 sensors. *Nat. Chem. Biol.* (2018). doi:10.1038/s41589-018-0168-3
- 874 30. Poelwijk, F. J., de Vos, M. G. J. & Tans, S. J. Tradeoffs and optimality in the  
875 evolution of gene regulation. *Cell* **146**, 462–470 (2011).
- 876 31. Yuen, C. M. & Liu, D. R. Dissecting protein structure and function using directed  
877 evolution. *Nat. Methods* **4**, 995–997 (2007).
- 878 32. Meyer, A. J., Segall-Shapiro, T. H. & Voigt, C. A. Marionette: E. coli containing  
879 12 highly-optimized small molecule sensors. *bioRxiv* 285866 (2018).  
880 doi:10.1101/285866
- 881 33. Libis, V., Delépine, B. & Faulon, J.-L. Sensing new chemicals with bacterial  
882 transcription factors. *Curr. Opin. Microbiol.* **33**, 105–112 (2016).
- 883 34. Eckert-Boulet, N., Pedersen, M. L., Krogh, B. O. & Lisby, M. Optimization of  
884 ordered plasmid assembly by gap repair in *Saccharomyces cerevisiae*. *Yeast*  
885 **29**, 323–334 (2012).
- 886 35. Xie, N.-Z., Liang, H., Huang, R.-B. & Xu, P. Biotechnological production of  
887 muconic acid: current status and future prospects. *Biotechnol. Adv.* **32**, 615–622  
888 (2014).
- 889 36. Havranek, J. J. & Harbury, P. B. Automated design of specificity in molecular

- 890 recognition. *Nat. Struct. Biol.* **10**, 45–52 (2003).
- 891 37. Carey, J. Gel retardation at low pH resolves trp repressor-DNA complexes for  
892 quantitative study. *Proc. Natl. Acad. Sci. U. S. A.* **85**, 975–979 (1988).
- 893 38. Choi, K. Y. & Zalkin, H. Structural characterization and corepressor binding of  
894 the Escherichia coli purine repressor. *J. Bacteriol.* **174**, 6207–6214 (1992).
- 895 39. Tovar, K., Ernst, A. & Hillen, W. Identification and nucleotide sequence of the  
896 class E tet regulatory elements and operator and inducer binding of the encoded  
897 purified Tet repressor. *Mol. Gen. Genet.* **215**, 76–80 (1988).
- 898 40. Gilbert, W. & Müller-Hill, B. Isolation of the lac repressor. *Proc. Natl. Acad. Sci.*  
899 *U. S. A.* **56**, 1891–1898 (1966).
- 900 41. Collier, L. S., Gaines, G. L., Neidle, E. L. & Neidle, E. L. Regulation of benzoate  
901 degradation in Acinetobacter sp. strain ADP1 by BenM, a LysR-type  
902 transcriptional activator. *J. Bacteriol.* **180**, 2493–2501 (1998).
- 903 42. Quijcho, F. A. & Ledvina, P. S. Atomic structure and specificity of bacterial  
904 periplasmic receptors for active transport and chemotaxis: variation of common  
905 themes. *Mol. Microbiol.* **20**, 17–25 (1996).
- 906 43. Roney, I. J., Rudner, A. D., Couture, J.-F. & Kærn, M. Improvement of the  
907 reverse tetracycline transactivator by single amino acid substitutions that reduce  
908 leaky target gene expression to undetectable levels. *Sci. Rep.* **6**, 27697 (2016).
- 909 44. Ezezika, O. C., Haddad, S., Clark, T. J., Neidle, E. L. & Momany, C. Distinct  
910 Effector-binding Sites Enable Synergistic Transcriptional Activation by BenM, a  
911 LysR-type Regulator. *J. Mol. Biol.* **367**, 616–629 (2007).
- 912 45. Craven, S. H. *et al.* Inducer responses of BenM, a LysR-type transcriptional  
913 regulator from Acinetobacter baylyi ADP1. *Mol. Microbiol.* **72**, 881–894 (2009).
- 914 46. Ruangprasert, A., Craven, S. H., Neidle, E. L. & Momany, C. Full-Length  
915 Structures of BenM and Two Variants Reveal Different Oligomerization  
916 Schemes for LysR-Type Transcriptional Regulators. *J. Mol. Biol.* **404**, 568–586  
917 (2010).

- 918 47. Ezezika, O. C., Haddad, S., Neidle, E. L. & Momany, C. Oligomerization of  
919 BenM, a LysR-type transcriptional regulator: structural basis for the aggregation  
920 of proteins in this family. *Acta Crystallogr. Sect. F Struct. Biol. Cryst. Commun.*  
921 **63**, 361–368 (2007).
- 922 48. Reichheld, S. E., Yu, Z. & Davidson, A. R. The induction of folding cooperativity  
923 by ligand binding drives the allosteric response of tetracycline repressor. *Proc.*  
924 *Natl. Acad. Sci. U. S. A.* **106**, 22263–22268 (2009).
- 925 49. Maddocks, S. E. & Oyston, P. C. F. Structure and function of the LysR-type  
926 transcriptional regulator (LTTR) family proteins. *Microbiology* **154**, 3609–3623  
927 (2008).
- 928 50. Bundy, B. M., Collier, L. S., Hoover, T. R. & Neidle, E. L. Synergistic  
929 transcriptional activation by one regulatory protein in response to two  
930 metabolites. *Proc. Natl. Acad. Sci. U. S. A.* **99**, 7693–7698 (2002).
- 931 51. Wang, M., Li, S. & Zhao, H. Design and engineering of intracellular-metabolite-  
932 sensing/regulation gene circuits in *Saccharomyces cerevisiae*. *Biotechnol.*  
933 *Bioeng.* **113**, 206–215 (2016).
- 934 52. Wang, L., Tang, H., Yu, H., Yao, Y. & Xu, P. An unusual repressor controls the  
935 expression of a crucial nicotine-degrading gene cluster in *Pseudomonas putida*  
936 S16. *Mol. Microbiol.* **91**, 1252–1269 (2014).
- 937 53. Gossen, M. & Bujard, H. Tight control of gene expression in mammalian cells by  
938 tetracycline-responsive promoters. *Proc. Natl. Acad. Sci. U. S. A.* **89**, 5547–5551  
939 (1992).
- 940 54. Guet, C. ;l C., Elowitz, M. B., Hsing, W. & Leibler, S. Combinatorial Synthesis of  
941 Genetic Networks. *Science* **296**, 1466–1470 (2002).
- 942 55. Bart, J. C. J. & Cavallaro, S. Transiting from Adipic Acid to Bioadipic Acid. Part  
943 II. Biosynthetic Pathways. *Ind. Eng. Chem. Res.* **54**, 567–576 (2015).
- 944 56. Karlsson, E., Mapelli, V. & Olsson, L. Adipic acid tolerance screening for  
945 potential adipic acid production hosts. *Microb. Cell Fact.* **16**, 20 (2017).

- 946 57. Swint-Kruse, L., Zhan, H., Fairbanks, B. M., Maheshwari, A. & Matthews, K. S.  
947 Perturbation from a distance: mutations that alter LacI function through long-  
948 range effects. *Biochemistry* **42**, 14004–14016 (2003).
- 949 58. Jensen, N. B. *et al.* EasyClone: Method for iterative chromosomal integration of  
950 multiple genes in *Saccharomyces cerevisiae*. *FEMS Yeast Res.* **14**, 238–248  
951 (2014).
- 952 59. Ambri, F., Snoek, T., Skjoedt, M. L., Jensen, M. K. & Keasling, J. D. Design,  
953 Engineering, and Characterization of Prokaryotic Ligand-Binding Transcriptional  
954 Activators as Biosensors in Yeast. *Methods Mol. Biol.* **1671**, 269–290 (2018).
- 955 60. Gietz, R. D. & Schiestl, R. H. Quick and easy yeast transformation using the  
956 LiAc/SS carrier DNA/PEG method. *Nat. Protoc.* **2**, 35–37 (2007).
- 957 61. Rosin, D., Hornung, G., Tirosh, I., Gispán, A. & Barkai, N. Promoter nucleosome  
958 organization shapes the evolution of gene expression. *PLoS Genet.* **8**,  
959 e1002579 (2012).
- 960 62. Mahr, R. *et al.* Biosensor-driven adaptive laboratory evolution of L-valine  
961 production in *Corynebacterium glutamicum*. *Metab. Eng.* **32**, 184–194 (2015).
- 962 63. Engohang-Ndong, J. *et al.* EthR, a repressor of the TetR/CamR family  
963 implicated in ethionamide resistance in mycobacteria, octamerizes cooperatively  
964 on its operator. *Mol. Microbiol.* **51**, 175–188 (2004).
- 965 64. Krissinel, E. & Henrick, K. Inference of macromolecular assemblies from  
966 crystalline state. *J. Mol. Biol.* **372**, 774–797 (2007).
- 967 65. Di Tommaso, P. *et al.* T-Coffee: a web server for the multiple sequence  
968 alignment of protein and RNA sequences using structural information and  
969 homology extension. *Nucleic Acids Res.* **39**, W13–7 (2011).

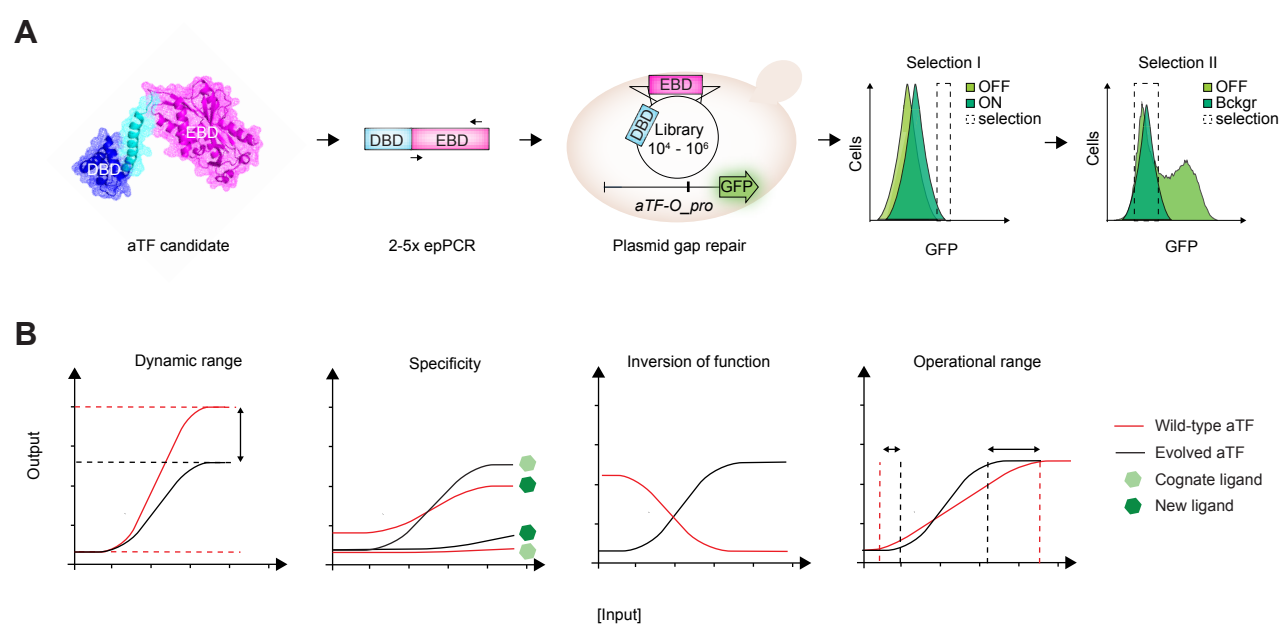
970

971

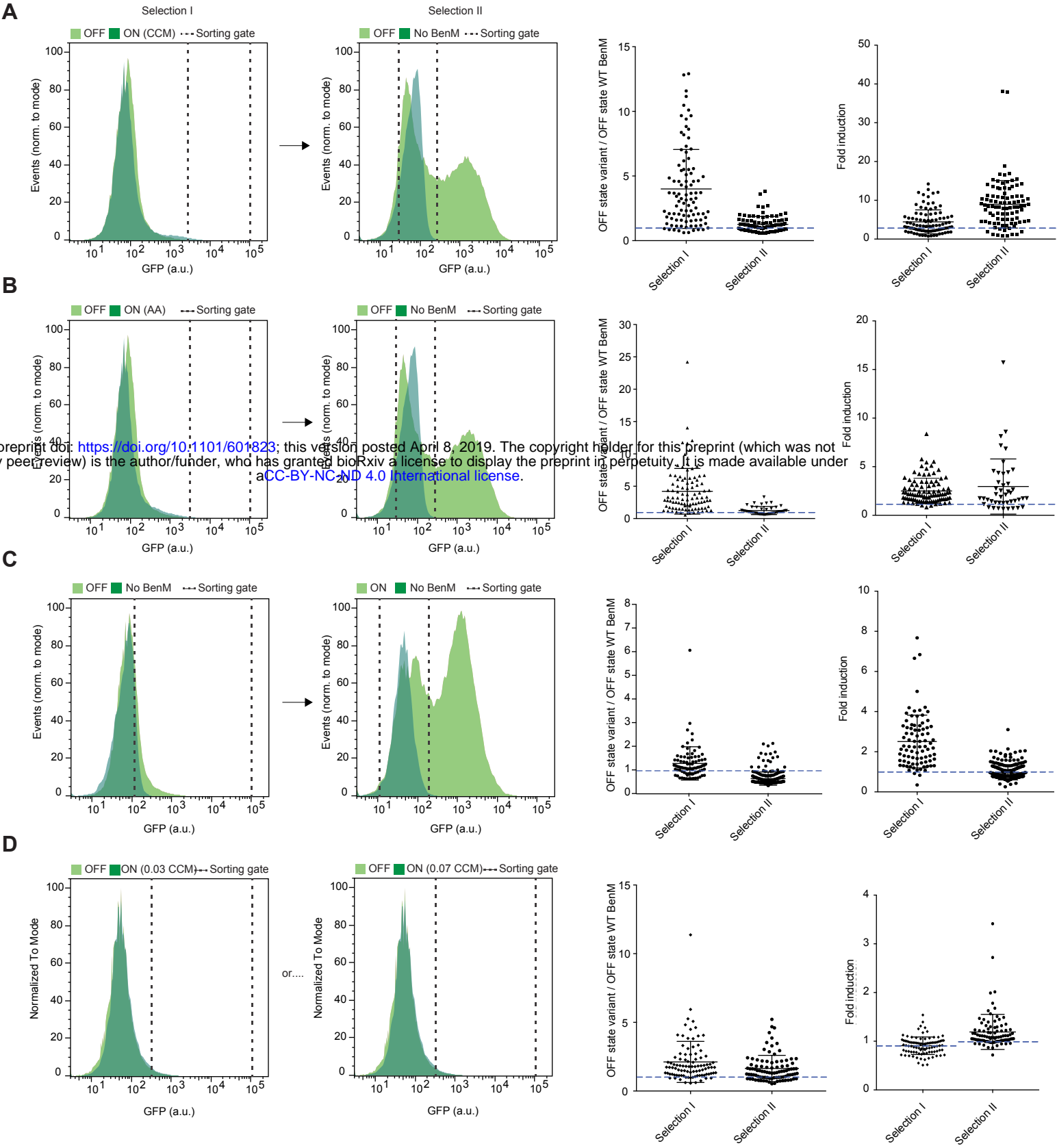
972



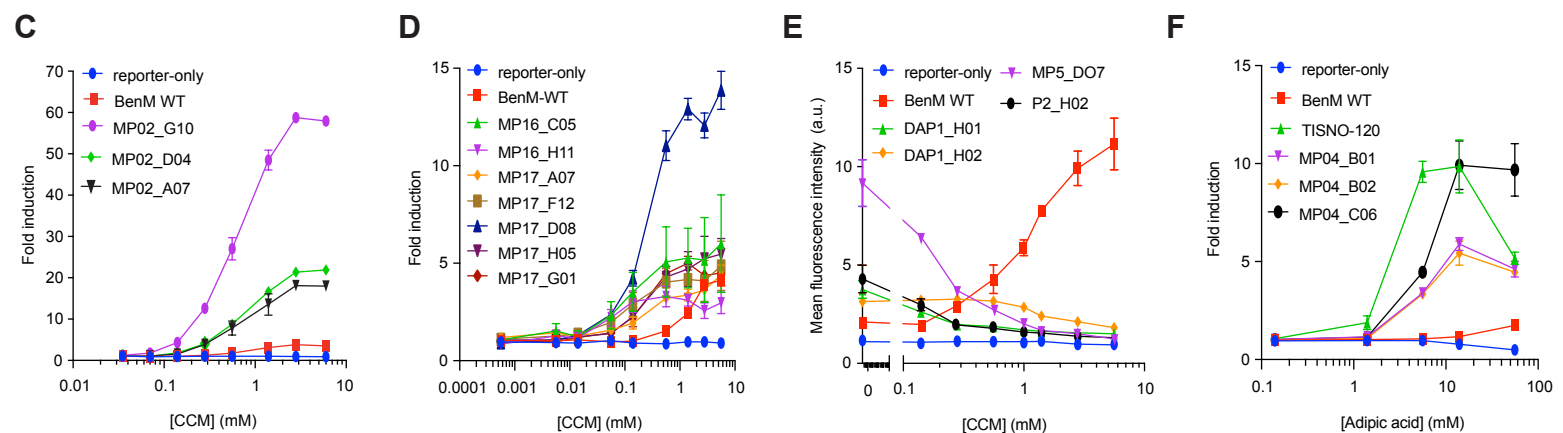




**Fig. 1. Outline of directed evolution workflow and toggled-based selection for user-defined biosensor transfer functions.**



**Fig. 2. Directed evolution of biosensor transfer functions by FACS-based toggled selection.**

[illegible]

**Fig. 3. Sequence-function analysis of evolved archetypical BenM variants.**

bioRxiv preprint doi: <https://doi.org/10.1101/601823>; this version posted April 8, 2019. The copyright holder for this preprint (which was not certified by peer review) is the author/funder, who has granted bioRxiv a license to display the preprint in perpetuity. It is made available under aCC-BY-NC-ND 4.0 International license.

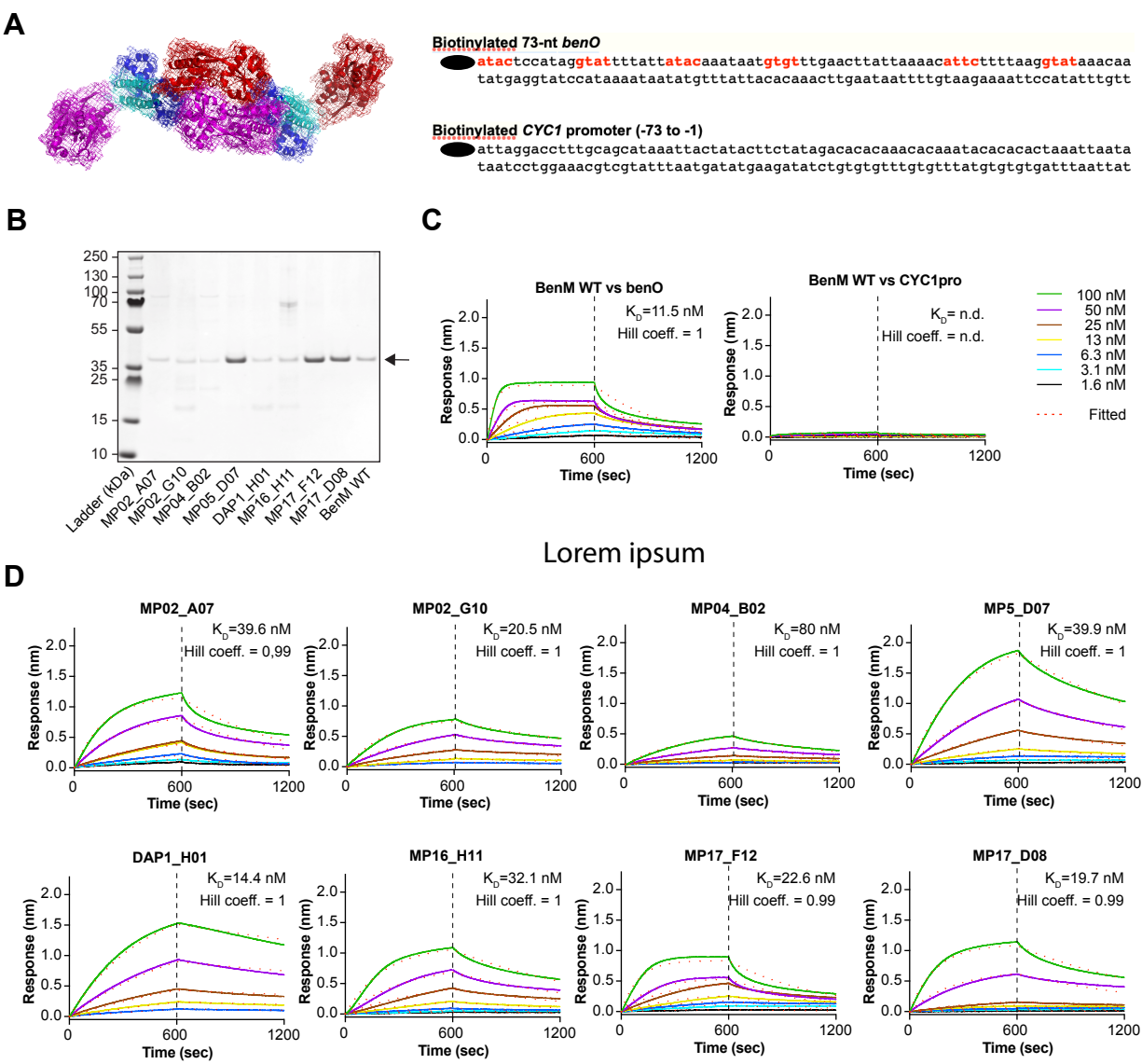


**Fig. 4. Biochemical charaterization of BenM and evolved archetypal variants.**

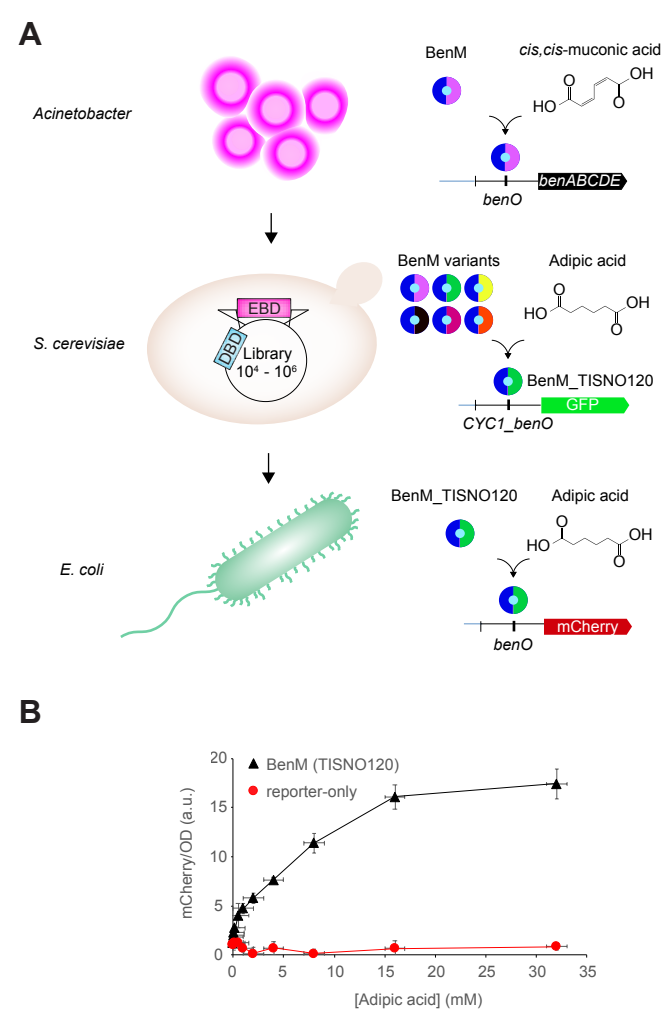


**Fig. 5. Host portability of evolved aTF biosensor variants.**